This chapter provides a description of MAR which is the regional climate model used in the thesis (Sect. 2.1). It also describes the large-scale forcings over the present and future periods (Sect. 2.2). This chapter also presents a new database that gathers near-surface climate (Sect. 2.3.1) and SMB observations (Sect. 2.3.2). This set of observations is based on pre-existing databases that were gathered together for the first time and also includes updates from more recent data. Finally, melt estimates used to evaluate MAR are also described (Sect. 2.3.3).

2.1   The regional climate model MAR

The "Modèle Atmosphérique Régional" (MAR) is a polar-oriented RCM firstly developed for representing katabatic winds over Terra Nova Bay (located in Victoria Land, East Antarctic; see Fig. C.2) in 1994 (Gallée and Schayes, 1994). The model has then also been used over the Greenland Ice Sheet (Gallée et al., 1995) before being adapted to temperate (De Ridder and Gallée, 1998; Brasseur et al., 1998) and tropical climate (Massager et al., 2004). Since those first studies, MAR has evolved to represent more physical processes and include many more parameterisations. The model is now recognised as a reference for simulating the climate and SMB of the two ice sheets (see Fettweis et al. (2020); Mottram et al. (2020)) and is also a member of several model intercomparison projects for instance over Belgium (e.g., Termonia et al., 2018) or the Arctic (e.g., Akperov et al., 2018; Inoue et al., 2021). The very first version of MAR only represented the atmosphere and after its interactions with the surface. This original atmosphere-land component has been recently coupled to both ocean and ice-sheet models leading MAR to rather an earth system model able to simulate interactions between atmosphere, ocean, and ice dynamics.

This section does not aim to retrace the history of the developpement of MAR or the parameterisations that have been included along with model developpements before being depreciated (we refer to the list of publications involving MAR available on https://mar.cnrs.fr/, last accessed 22/01/2021), but to present the model in its current state (MARv3.11) and undocumented changes. Moreover, the description of MAR in the next sections would be more exhaustive

than frequently needed for ensuring a general comprehension of how the model works. They have therefore been constructed with several levels of readings for each aspect of the model from summary to in-depth descriptions.

MAR, as most current atmospheric models (whether for climatological or meteorological applications), is composed of 1) a dynamical core that solves the primitive and known equations of the atmosphere and 2) a physical heuristic core for all the processes not represented by the dynamical core. Although the primitive physical equations representing the conservation of mass, momentum, and (heat) energy) are shared by the different models, their mathematical expression mainly depends on approximations and numerical methods used by each model. The dynamical core is the part of the model code that simulates the large-scale and horizontal movements. The physical core and the included parameterisations of a model aim to represent the effects of processes not resolved by the dynamical core on the energy source terms in the primitive equations within the 1D atmospheric column through heat exchanges by radiation, water-phase changes, interactions with the surface, or subgrid-scale movements (turbulence, convection). This second part is based in particular on a combination of physical equations and conservation laws, theories, empirical and semi-empirical parameterisations. This is a strong source of spread between models and can be regarded as the main strength of a regional model like MAR that seeks to represent in detail the processes specific to a given area. The chapter is thus organised as follows: a brief presentation of the dynamic core of MAR and the numerical methods used (Sect. 2.1.1), the nudging methods (Sect. 2.1.2) and a more exhaustive presentation of the physics of MAR (Sect. 2.1.3).

2.1.1 Dynamical core

MAR is a hydrostatic model that solves the primitive equations as described in Gallée and Schayes (1994). The mass conversion equation is expressed in its full continuity form without approximation. In order to better represent topography-induced variations in the atmosphere, the vertical coordinate (σ_{level}) is normalized by the presure (Eq. 2.1):

$$\sigma_{level} = (p - p_{top})/(p_s - p_{top}) \tag{2.1}$$

where p, p_{top}, and p_{top} are respectively the level pressure, the surface pressure and a constant pressure at the top of the atmosphere (p_{top}= 0.1 hPa in most current

MAR configurations).

The model also takes into account the air loading (Eq. 2.2, adapted from Gallée (1995)) due to hydrometeor particles (see subsect. 2.1.3.1 for the descriptions of hydrometeors in MAR) in the air specific mass (air density) by changing the virtual temperature and the hydrostatic equation.

$$Loading = 0.85 \times (q_v - 1.64 \times (q_w + q_i + q_r + q_s)) \tag{2.2}$$

where q_v, q_w, q_i, q_r, q_s are the specific humidity concentration ($\mathrm{kg\,kg^{-1}}$), and the concentrations ($\mathrm{kg\,kg^{-1}}$) of cloud droplets, ice crystals, rain droplets, and snow particles.

The numerical scheme relies on a spatial discretisation based on Arakawa A grid (Arakawa and Lamb, 1977). It solves differential equations of horizontal momentum and conservation using finite differences and more especially a numerical centered scheme, second-order-accurate (leap-frog) in time and fourth-order accurate in space (Gallée and Schayes, 1994). This scheme computes the new values at distinct interleaved time steps using different levels of precision for time and space. The advection is handled by a semi-Lagrangian scheme adapted from Pielke (1984) and improved by Seibert and Morariu (1991) that represents a compromise between the Eulerian fixed frame and the Lagrangian parcel frame of reference. Wind-components (u,v), specific humidity and potential temperature are filtered using a two-dimension low-pass filter (Raymond and Garder, 1988). In the same way, the mass conservation equation is corrected following the relaxation term defined by Yan and Anthes (1987) to limit mass changes in open-boundary conditions. Finally, MAR is parallelised using the application programming interface Open-MP (Fettweis et al., 2017).

2.1.2   Nudging and boundaries

As MAR only simulates atmospheric processes and their interactions with the surface over a regional area, the model has to be constrained at its boundaries by large-scale forcing fields. These forcings mainly come from two different kinds of models: reanalyses and GCMs or ESMs. A reanalysis is a climate model that associates a dynamical core and physical-process representations (as does MAR) with different levels of complexity of data (observation) assimilation. GCMs and ESMs are also climate models representing the Earth's climate but without

assimilation methods, mainly used to study past and future climate variations. We refer to Sect. 2.2 for a more detailed description of the large-scale forcings used in this manuscript.

The boundary conditions enable to take into account the contribution of larger (global) meteorological processes and climate variability. The integration domain is divided in 3 areas (Fig. 2.1). At the lateral boundaries, the MAR results are prescribed by the large-scale forcing field values, while inside the domain it does not assimilate any observations or values from the large-scale forcing to drive its results. The 7-pixel transition between these two areas (the relaxation zone) aims to progressively make the model solution independent of the large-scale forcing. MAR is forced by 6-hourly lateral conditions and a linear interpolation is made at each model time step to ensure a smooth temporal transition from the current forcing to the next one.
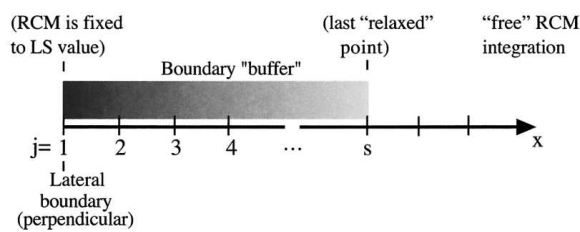

Figure 2.1: Schematic view of the boundary treatment reproduced from Marbaix et al. (2003)

The dynamic relation includes a Newtonian term (following Davies (1976)) and a diffusion term (Davies, 1983; Anthes et al., 1989). The Newtonian term removes a part of the difference between the MAR results and its forcing while the second term diffuses the differences horizontally. We refer to Marbaix et al. (2003) for more details about the lateral nudging of MAR.

The relaxation method described above is only applied at the lateral boundaries where MAR is constrained by the surface pressure (influencing the vertical discretisation), temperature, specific humidity, and both u-v wind components from the large-scale model. It then does not directly assimilate neither clouds nor precipitation. Since MAR does not represent the ocean (except in coupling experiments such as in Jourdain et al. (2011), it is also forced by SCCs: SST and SIC. For these two variables, there is no buffer zone as above and MAR is entirely forced by SST and SIC from the large-scale fields.

MAR has firstly been developed to simulate the climate of local areas. It then adds small-scale values in its results while the general circulation is supposed

to remain the one prescribed by the large-scale forcing. For larger domains (such as over the AIS or the Arctic), MAR has a greater degree of freedom due to a larger modelled area. To prevent it from creating its own atmospheric circulation and better constraining the climate variability by the large-scale forcing, an additional nudging was added at the top of the atmosphere following van de Berg and Medley (2016). This nudging is qualified to be an indiscriminate forcing as it adjusts MAR results to the large-scale fields without considering spatial scales or structures (as opposite to spectral nudging). Although this one removes a fraction of MAR small-scale patterns not represented in the coarser-resolution large-scale forcing, it combines both the added value from the RCM and the interannual variability from its forcing in the upper layers of troposphere ($\geq 200\text{hPa}$) and stratosphere. The upper air relaxation used in MAR (Agosta et al., 2019) is only applied on temperature and u-v wind components in the higher atmospheric levels. The upper specific humidity is not nudged to prevent any impact on the cloud microphysics of the model. Furthermore, the upper air relaxation is stronger at the top of the model while gradually decreasing for underneath layers. Due to the sigma coordinates, the relaxation never directly changes the near-surface fields even in case of strong topography variations (van de Berg and Medley, 2016).

2.1.3 Model physics

2.1.3.1 Cloud-microphysical scheme

The model includes a cloud-microphysical scheme solving conservation equations for the concentration of five water species (cloud droplets (q_w), ice crystal (q_i), rain drops (q_r), snow particles (q_s), and specific humidity (q_v) firstly described by Gallée (1995)) and the ice crystal number(n_i) (Massager et al., 2004). MAR solves the conservative equation 2.3 for every horizontal pixel and vertical-σ layer.

$$\frac{\delta q_\alpha}{\delta t} = -u \cdot \frac{\delta q_\alpha}{\delta x} - v \cdot \frac{\delta q_\alpha}{\delta y} + \dot{\sigma} \cdot \frac{\delta q_\alpha}{\delta \sigma} + F_{q\alpha} + P_{q\alpha}(+P_{sed}) \qquad (2.3)$$

where the three first terms represent the 3D advection by the wind following the x, y and σ directions, $F_{q\alpha}$ the turbulent flux divergence of the hydrometeor specie, and P_{sed} a source term. P_{sed} is an additional term that describes the sedimentation of precipitating hydrometeors (rain drops, snow particles, and ice crystals) depending on their specific falling velocities. The source term in Eq. 2.3 represents the 21 microphysical processes detailed in Table 2.1 originally based

on Kessler (1969) parameterisations in addition to the sedimentation towards the surface of the three precipitating hydrometeors. Since graupels are not (fully yet) included in the model, all accretion processes that should result in graupel following Lin et al. (1983) lead to snowflake formation assuming a Marshall-Palmer size distribution (Gallée, 1995).

Table 2.1: Microphyscal processes represented in MAR and associated references as firstly described by Gallée (1995) and modified afterwards

Nucleation by cloud droplet solidification (q_w to q_i, if $TT \leq -35$ °C)	Emde and Kahlig (1989); Levkov et al. (1992)
Deposition and condenstation-freezing nucleation (q_v to q_i, if $TT \leq -35$ °C)	Meyers et al. (1992); Levkov et al. (1992)
Contact-freezing nucleation or depositional growth of cloud ice (q_w to q_i)	Meyers et al. (1992); Prenni et al. (2007); Levkov et al. (1992)
Ice crystal sublimation (q_i to q_v)	Emde and Kahlig (1989); Levkov et al. (1992)
Ice crystal melting (q_i to q_w, if $TT \geq 0$ °C)	Levkov et al. (1992)
Water vapor condensation (q_v to q_w, if $TT \geq -35$ °C)	Emde and Kahlig (1989)
Cloud droplet evaporation (q_w to q_v)	Emde and Kahlig (1989)
Cloud droplet autoconversion (q_w to q_r)	Lin et al. (1983); Sundqvist (1988)
Depositional growth of snow (q_i to q_s)	Levkov et al. (1992)
Ice crystal aggregation (q_i to q_s)	Levkov et al. (1992)
Accretion of cloud droplet by rain (q_w to q_r)	Lin et al. (1983); Emde and Kahlig (1989)
Accretion of cloud droplet by snow (q_w to q_s)	Lin et al. (1983); Locatelli and Hobbs (1974)
Accretion of ice crystal by snow (q_i to q_s)	Lin et al. (1983); Levkov et al. (1992)
Accretion of ice crystal by rain (since no graupel, q_i to q_s, if $TT \leq 0$ °C)	Lin et al. (1983); Levkov et al. (1992)
Accretion of rain by ice crystal (since no graupel, q_r to q_s, if $TT \leq 0$ °C)	Lin et al. (1983)
Accretion of rain by snow (since no graupel, q_r to q_s, if $TT \leq 0$ °C)	Lin et al. (1983); Emde and Kahlig (1989)
Accretion of snow by rain (since no graupel, q_s to q_r, if $TT \geq 0$ °C)	Lin et al. (1983); Emde and Kahlig (1989)
Rain freezing (since no graupel, q_r to q_s, if $TT \leq 0$ °C)	Lin et al. (1983); Emde and Kahlig (1989)
Rain evaporation (q_r to q_v)	Lin et al. (1983)
Deposition on snow (q_v to q_s) or sublimation (q_s to q_v)	Lin et al. (1983)
Snow melting (q_s to q_r, if $TT \geq 0$ °C)	Lin et al. (1983)
Rain sedimentation	Emde and Kahlig (1989)
Snow sedimentation	Emde and Kahlig (1989); Levkov et al. (1992); Locatelli and Hobbs (1974); Fettweis et al. (2017)
Ice crystal sedimention	Levkov et al. (1992)

Table 2.1 also lists the parameterisations that have been recently included in MAR since the original description by Gallée (1995). In particular, the ice crystal nucleation used by Lin et al. (1983) (and based on Fletcher (1962) overestimates ice crystal concentration leading to the model underestimation of the downwelling solar radiation towards the surface, the convective available potential energy (CAPE), and rain (Massager et al., 2004). It has thus been replaced by Meyers et al. (1992)'s parametrization later improved by Prenni et al. (2007). Ice crystal sedimentation is not neglected anymore by adding a prognostic equation for ice crystal number according to Levkov et al. (1992). Furthermore, the conversion rate of cloud droplets to rain particles takes into account an adapted parameterisation from Sundqvist (1988). It relies on two parameters: a critical cloud water mixing ratio (qwo) enabling the rainfall formation and a characteristic time scale for auto-conversion processes (CO). Note that a low fraction of cloud droplets can be converted to rain even if q_w is lower than qwo (Delobbe and Gallée, 1998). In MARv3.11, qwo and Co values are respectively fixed to $1 \cdot 10^{-3}$ (kg kg^{-1}) and $1 \cdot 10^{-4}$. Finally, other subtle adjustments such as an increase in snowfall sedimentation velocity or cloud lifetime (Fettweis et al., 2017, 2020) have been made to tune the model in order to more accurately reproduce clouds over the polar ice sheets.

2.1.3.2   Radiative scheme

The radiative scheme is composed of two individual shortwave and infrared schemes as detailed in Morcrette (2002). MAR uses the radiative scheme from the ECMWF ERA40 reanalyses Uppala et al. (2005).

The shortwave radiation scheme (Fouquart and Bonnel, 1980) has been updated by Morcrette (1993). It solves the shortwave transfer equation by using a two-stream method that accounts for the scattering (due to clouds and aerosols) following a Delta-Eddington approximation (Joseph et al., 1976). For each atmospheric layer, the transmission and reflectivity depends on 1) scatterings by molecules (Rayleigh scattering), aerosols, and clouds; 2) absorptions by gases, aerosols and clouds; 3) reflection by the surface (Morcrette, 2003). Water vapour, uniformly-mixed gases (CO_2, O_2 in the original version and CH_4, $N_2 0$, CO as updated by Morcrette (1993)), and ozone (with a function of the effective zenith angle) are taken into account, as well as the temperature and the pressure. Following Morcrette (1993), the shortwave downwelling radiation (SWD) reaching the surface is particularly dependent on the aerosol concentration. Finally, the Fouquart and Bonnel's scheme determines the transmission and reflectivity for clear-sky and cloudy conditions separately assuming maximum-random cloud overlap. The scheme assumes that all cloud layers maximise their vertical overlap and that each cloud layer is treated independently (See Morcrette and Fouquart (1986) for the sensitivity of the radiative scheme to this assumption).

For the longwave radiation scheme, MAR uses an improved version (Morcrette et al., 2003) of the Rapid Radiation Transfer Model (Mlawer et al., 1997) based on the correlated-k method. This method is an approximate technique that enables fast computations of radiative fluxes and cooling rates for non-homogeneous atmospheres using limited approximations. The continuous infra-red spectrum is divided in several discrete bands. Each band corresponds to a small spectrum window where a limited number of gases (2 in this scheme) could strongly absorb the energy. The absorption due to these gases is modelled with a high precision, while the other gases (considered to be minor absorbers) are less rigorously taken into account. Represented species are water vapour, CO_2, O_3, CH_4, N_2O and the main halocarbons (CFC-11, CFC-12, CFC-22, CCl-4) (Mlawer et al., 1997). Similarly to the shortwave scheme, the longwave scheme includes a maximum-random overlap assumption (Morcrette, 2002).

Both improved shortwave and longwave radiation schemes represent the in-

teractions (absorption, attenuation, scattering, and reflection) between hydrometeors computed by the cloud-microphysical scheme and radiations. The radiative scheme uses q_i, q_w, and q_v concentrations from each atmospheric layer to determine the cloud optical properties. The latests depend on the region of the solar spectrum and on the particle phase contained in the cloud. Since properties of mixed phase clouds (containing both liquid and ice particles) are the summed contribution of both phases (Morcrette, 1993), the two next paragraphs will describe the individual contribution of ice and water particles on shortwave and longwave cloud optical properties.

For shortwave radiations, the scheme uses the microphysical properties defined by Slingo (1989) for water clouds and by Fu (1996) for ice clouds. Slingo's parameterisation links water cloud properties with the cloud liquid water path (vertically-integrated water content between the cloud base and top) and equivalent droplet-radius size distribution neglecting the effect of water vapour. In the same way, the shortwave optical properties for ice clouds are defined on the ice water content and the generalised effective size that represents the ice-crystal size distribution. In a few words, smaller ice particles have a higher radiative effect resulting notably in more scattering and absorption than larger ice particles (Morcrette, 1993).

Similarly, the water cloud properties for longwave is a function of the liquid water content vertically-integrated over the layer (liquid water path) and the effective radius based on the droplet size distribution as described by Lindner and Li (2000). This parameterisation neglects scattering interactions which makes absorption the dominant processes for longwave radiation. Optical properties for ice particles in the longwave spectrum are functions of the cloud ice water content and generalised effective size that accounts for different ice crystal distributions (Fu et al., 1998). Furthermore, the radiative scheme used by MAR also enables the use of different parameterisations to compute the cloud optical properties. Morcrette (2002) suggested a relatively low effect on longwave but a higher effect (up to 10 unitW m^{-2}) on the shortwave in cloudy conditions.

The radiative transfer relies on the effective radius which is a factor describing the distributions of the mass and volume of the particles. The ice effective radius is computed using Sun and Rikus (1999) parametrization and is a function of the ice-water content and cloud temperature. It has been adapted to Antarctic conditions using a value of 15 µm as the minimum diameter for ice particles (Walden et al., 2003). The liquid effective radius is a linear function of the

liquid water content and the droplet water concentration contained in the cloud depending on the continental or oceanic origin of the air masses (Martin et al., 1994) which in MAR is simply depending on the land-sea mask.

As highlighted above, radiative cloud properties do not directly depend on q_s concentration. The q_s concentration is implicitly taken into account by being partially included in the q_i concentration from each layer treated by the radiative scheme. The contribution of q_s is expressed as an additional mass for q_i by assuming that the total ratio of q_s and q_i is similar to the ratio of effective radii, i.e only 30% of q_s is added in q_i seen by the radiative scheme (Gallée and Gorodetskaya, 2010). The effect of rain droplets on radiations is neglected. This assumption is reasonable knowing that the fall velocity of rain droplets used in MAR (Emde and Kahlig, 1989) induces that most of them reach the surface within one time-step of the radiative scheme.

Gas concentration are provided by historical concentration, in particular the MAR radiative scheme uses the Fortuin and Langematz (1995)'s ozone climatology. Future concentration are specified by the selected emission pathway, i.e the Representative Concentration Pathway (RCP) (Moss et al., 2010) used for the latest IPCC report or the more recent Shared Socioeconomic Pathways (ssp) (O'Neill et al., 2016) that represents future emissions for different socio-economic trajectories. Note that while the cloud mycrophisical scheme uses a constant aerosol value (Meyers et al., 1992), the aerosols inputs of the radiative scheme are time-varying loads based on a monthly climatology of tropospheric aerosols (soil dust, sulfate, sea salt, black carbon, and organic) defined by Tegen et al. (1997) and daily volcanic aerosols from the Goddard Institute for Space Studies. Only the present observed aerosol-radiation interactions till 2002 are taken into account in MAR since cloud-aerosols interactions are neglected (Wyard et al., 2018).

2.1.3.3 Convective scheme

The hydrostatic approximation used by MAR implies that other vertical forces are negligible compared to pressure forces (Archimede) and weight. This means that only relatively small vertical movements due to small (smoothed) topography variations are permitted. In other words, vertical movements are negligible compared to horizontal movements. This is suitable for representing the large-scale katabatic flow. This limits the horizontal resolution over complex-topography areas such as the Antarctic Peninsula where strong vertical topographic

gradients at very high resolution could induce strong vertical updrafts and make the approximation invalid; but also requests an implicit representation of large vertical movements that occurs during convective events. Cold conditions in Antarctica prevent the development of strong convective movements, but yet enables convection to occur (Van Den Broeke et al., 2006; Van Wessem et al., 2014a; Kuipers Munneke et al., 2018). Furthemore, a low amount of precipitation over coastal areas can be generated by convective clouds (Van Wessem et al., 2014b).

The convection in MAR is based on an updated version of the convective scheme from Bechtold et al. (2001) used in MESO-NHv5.3.1 (Lac et al., 2018). The parameterisation is a bulk mass-flux that represents the deep and shallow convections. It represents moist thermodynamics and convective downdraughts as well as dry thermals. If the temperature of at least one atmospheric layer is higher than -3°C, or if there is no temperature inversion in the near-surface levels and the near-surface temperature exceeds 10°C at night, the convective scheme determines whether the atmospheric profile is unstable. If the profile is considered as unstable, the convective scheme tries to restore an equilibrium by implicitly representing vertical mouvements and by inducing hydrometeor concentration and temperature changes. In the case of the scheme used by MAR, the equilibrium is assumed to be restored when 90% of the convective available potential energy has been removed (Bechtold et al., 2001). Two types of different convections are explicitly represented: shallow and deep convections that differ in the size of the clouds (>500 m and >3000 m) and the characteristic time-scale (shallow between 1h and 3h and deep between 30 min and 1h). The deep convection scheme is based on Kain and Fritsch (1990) that also represent the convective clouds (Lac et al., 2018). The scheme predicts the temporal evolution of atmosphere quantities (notably momentum, temperature, and hydrometeor concentrations) as well as liquid and solid precipitation engendered by the convective adjustments.

Since convective precipitation is assumed to instantaneously reach the surface, their interactions with the surrounding atmosphere is only accounted for in the convective scheme. This means that rain and snowfall computed by the convective scheme follow different processes than the ones described in Sect. 2.1.3.1. In the same way, they are not included in the quantities seen by the radiative scheme. Doutreloup et al. (2019a,b) evaluated the effect of using different convective schemes in MAR to represent present and future rainfall in Belgium and found significant differences in modelled precipitation although no scheme resulted in a

better representation of precipitation than another one.

2.1.3.4 Turbulence scheme

Similarly to convective movements, subgrid-scale and high-frequency turbulent movements cannot be directly represented by the model. This means that parameterisations are needed to represent heat, momentum, and hydrometeor transfers. Subgrid-scale fluxes are parameterised differently in the surface boundary layer and above it. The turbulence in MAR has been particularly developed to represent very stable conditions that can be found over the ice sheets (Duynkerke, 1991; Duynkerke and Van den Broeke, 1994).

The turbulence above the surface boundary layer is modelled using the one-and-half order closure $E - \epsilon$ model by Duynkerke (1988) and updated by Bintanja (2000) for taking into account the sedimentation of snow particles. It includes prognostic equations for turbulent kinetic energy production (E) and turbulent kinetic energy dissipation (ϵ). The turbulent mixing length then depends on the local flow characteristics which is important for representing the katabatic winds (Gallée et al., 2001). The turbulence also depends on water phase changes (Duynkerke and Driedonks, 1987).

In the surface boundary layer, the parametrization of subgrid-scale fluxes is based on Monin-Obukhov similarity theory using stability functions described in (Duynkerke and Van den Broeke, 1994). MAR also represents the increase in air density due to the presence of snow by changing the virtual potential temperature used in the turbulent scheme.

Furthermore, MAR represents the small-scale exchanges between sea sprays and the near-surface atmosphere. The projected water enhances evaporation acting as a moisture source over the ocean and decreasing the air potential temperature. These exchanges are parameterised as a function depending on the fraction of open ocean and the near-surface wind speed (Andreas, 1990, 1995; Andreas and Emanuel, 2001; Andreas and Decosmo, 2002; Andreas, 2004).

2.1.3.5 Surface module

One of the MAR strengths is its ability to represent the interactions between the atmosphere and the surface, but also the evolution of the properties of the soil, the vegetation, and especially the snowpack. The transfer of mass and energy

between the surface and the atmosphere is simulated by the 1-D surface scheme SISVAT (Soil Ice Snow Vegetation Atmosphere Transfer) module, which consists of soil and vegetation (De Ridder and Schayes, 1997; De Ridder, 1997), snow (Gallée and Duynkerke, 1997; Gallée et al., 2001) and ice (Lefebre et al., 2003) sub-modules.

For MAR and SISVAT, each surface pixel is either fully oceanic or continental (including the floating Antarctic ice shelves). However, the surface pixel in SISVAT includes a tilling that divides the surface pixel in several sub-pixels in order to better represent the heterogeneity of surface conditions. Oceanic pixels can then be open-ocean, ice-covered, or any combination of both conditions (Gallée, 1996). Similarly, continental pixels are divided into three subpixels representing several types of vegetations (De Ridder and Gallée, 1998) for temperate and tropical climate configurations of MAR, or in two surface subpixels for the permanent ice and tundra (Fettweis et al., 2013) in polar configurations, excepted over the AIS where the surface is composed of permanent ice and exposed rocks called Nunataks (Kittel et al., 2020). SISVAT is called for each subpixel and MAR averages momentum and energy fluxes using weighting coefficients according to the sub-pixel fraction (De Ridder and Gallée, 1998). SISVAT is forced by atmospheric variables from the nearest surface level (wind speed, temperature, humidity, precipitation, and both downwelling shortwave and longwave fluxes) to compute turbulent (latent and sensible) fluxes, reflected shortwave and emitted longwave radiations.

Soil and vegetation

The soil and vegetation modules (De Ridder and Schayes, 1997) describe the properties of 7 soil vertical layers and one vegetation layer, and resulting transfers with the atmosphere. There are 12 types of vegetation (and a 13th that represents urban area) which have different properties of albedo, emissivity, and evaporation capacity. Although the "vegetation" classes are not used in the Antarctic configuration of MAR, the vegetation module will be described for the sake of completeness in the next paragraphs and because it is closely related to the soil module.

The modules solve the energy and water balances separately for the soil and vegetation. In SISVAT, both the vegetation and soil are considered to be directly ventilated by the turbulence which means that direct exchanges between the ground and the canopy are neglected (De Ridder and Schayes, 1997). The sensible heat flux is then computed as the sum of the ground and vegetation

contributions, while the latent heat flux is also the sum of both these contributions (evapotranspiration and ground depending on the soil humidity potential) and the direct contribution of evaporation in case of wet leaves.

The vegetation is described with several properties which facilitate or mitigate the canopy transpiration and which absorb or reflect more radiations. The transpiration depends on differences in water potential between the soil and the leaves that regulate the flow from the ground to the atmosphere through the canopy. It takes into account the soil-root resistance and the number of roots fraction in the upper soil (De Ridder and Schayes, 1997). Each vegetation type has its own stomatal resistance to represent leaf properties and resulting resistance compared to radiation, water stress, temperature or humidity saturation deficit. Monthly climatology of the Leaf area index (LAI) from the MERRA-2 reanalysis (Gelaro et al., 2017) are used to determine the stomatal resistance and inherent transpiration, the heat vegetation capacity (Gallée and Duynkerke, 1997) and interactions with solar radiations (De Ridder, 1997). In addition to LAI, the canopy surface energy budget takes into account zenith and azimuth angles, and reflective/absorptive properties of the different vegetation classes. SISVAT also represents multiple shortwave scattering due to multiple leaf-interactions and the longwave emission trapping inside the canopy that result in a higher canopy emissivity than the emissivity of a single leaf (De Ridder, 1997). Furthermore, the canopy layer acts as a supplementary layer above the ground for radiations (De Ridder, 1997).

In the soil and vegetation modules in SISVAT, the liquid water can either be pumped towards the surface by the evapotranspiration of the ground and the canopy, or percolate into the ground. The diffusion-gravitation equation that represents the transport of liquid water into the soil is based on the soil water content that determines the soil water potential and hydraulic conductivity following (Clapp and Hornberger, 1978) and the soil hydraulic diffusivity (Hillel, 1971). When the liquid water (rain and snow melting) amount exceeds the maximum infiltration rate, the extra water is assumed to runoff and is considered to be lost for the soil water balance in the absence of a river scheme.

Rocks (nunataks or non-snow-covered ground) and surface open-ocean are considered as two different soil classes in SISVAT. The soil heat capacity depends on the soil substrates and water content. Ocean is considered permanently saturated in water. Exposed rocks have a low albedo (0.17) contrasting with the prevailing high albedo of the snow over the AIS. The open-ocean albedo is fixed at

0.11. Open-ocean roughness length for momentum and heat follows Wang (2001) while the soil roughness length for rocks is a fixed value (0.01).

Ice and snow

The dynamical snow and ice components represent snow properties and metamorphism across 30 snow/firn/ice layers resolving the 20 first meters of snow/ice over the ice-sheet pixels. In SISVAT, sea ice potentially covered by snow is represented with the same processes as the snow/ice on the ice sheet. While the snow/ice height is kept fixed over the AIS, the sea-snow/ice thickness is constrained by th e presence of sea ice in the large-scale forcing. For each surface pixel with a SIC value greater than 0%, the MAR sea-ice thickness is initially fixed at 55 cm and sea ice can be covered by snow. The sea-ice thickness can then evolve as a function of accumulated snowfall or surface melt, with a minimum thickness of 10 cm as long as the forcing SIC is positive. Similarly, the snowpack height over rocks changes according to snow accumulation or erosion without any minimal thickness.

The snow and ice module consists of the physical snowpack model of (Gallée and Duynkerke, 1997) and a former version of CROCUS (Brun et al., 1989) with snow metamorphism laws (Brun et al., 1992). The metamorphism laws describe the snow grains in terms of dendricity, sphericity, and descriptive size. The fresh-fallen snow has a dendricity around 1 and decreases to 0 representing the part of original crystal shapes that are still in a snow layer. Sphericity (0-1) represents the ratio of rounded shapes compared to angular and evolves according to temperature gradients between the snow layers. Large (small) gradients result in decreased (increased) sphericity.

The snowpack is also described through other physical parameters: temperature, liquid water content, and density. Over the AIS, the density of the fresh falling snow (Eq. 2.4) is a function of the $10\,\mathrm{m}$ wind speed ws_{10} ($\mathrm{m\,s^{-1}}$) (adapted from Agosta et al. (2019) in Kittel et al. (2020) to fit density observations over the upper 50 cm (Agosta et al., 2019, Table S2):

$$\rho_\mathrm{s} = 200 + 32 \cdot \mathrm{ws}_{10}, \tag{2.4}$$

with minimum and maximum values fixed to 300 and $400\,\mathrm{kg\,m^{-3}}$. The dry snow settling is parameterised as a function of the weight of overlying layers and effect of metamorphism (described in Gallée and Duynkerke (1997) following Navarre (1975)). Densification also occurs as a consequence of melt and refreezing into

the snowpack that promotes grain cohesion and decreases the firn air content. In MAR, the snow is assumed to have density values between $300\,\mathrm{kg\,m^{-3}}$ and $450\;\mathrm{kg\,m^{-3}}$ while ice has a minimal density of $830\,\mathrm{kg\,m^{-3}}$. Between these two types is the firn ($450\,\mathrm{kg\,m^{-3}}$ – $830\,\mathrm{kg\,m^{-3}}$).

Sea-ice and ice-sheet surfaces have the same thermal and texture properties. The snow-conduction coefficient is a function of the density Yen (1981) while the snow-heat capacity is fixed at $2105\,\mathrm{J\,kg^{-1}\,K^{-1}}$ (Loth et al., 1993) and emissivity of the snow is 0.99. In MARv3.11, the roughness length for momentum z_{0m} is fixed at 1 mm but can also be a function of the air temperature as in the previous model version (Agosta et al., 2019) and used for Ch. 4. The contribution of the subgrid orography can be included in the roughness length computation (Jourdain and Gallée, 2011) but is deactivated as it requires a resolution-dependant tuning. Finally, melt (through increase in snow/ice density) influence is not taken into account in contrast to the Greenland configuration (Greuell and Konzelmann, 1994; Lefebre et al., 2003). The roughness length for heat z_{0t} is often derived from z_{0m} using a scaling factor ranging from 1-100 (Garratt, 1992). In MAR, z_{0t} equals z_{0m} scaled by 7.4 linking the two properties with the Reynolds number (Andreas, 1987) although no universal relation has proved yet to be efficient over the AIS (see Vignon et al. (2017) and references therein).

SISVAT resolves the energy and water budget for each layer of the snowpack that leads to changes in temperature and humidity content. The snow-covered surface energy budget (SEB, Eq. 2.5) is defined as:

$$SEB = SWN + LWN + SHF + LHF + G, \tag{2.5}$$
$$SWN = SWD - SWU, \tag{2.6}$$
$$SWU = \alpha \times SWD, \tag{2.7}$$
$$LWN = LWD - LWU, \tag{2.8}$$
$$LWU = \varepsilon \times \sigma \times ST^4, \tag{2.9}$$

with SEB the surface energy budget, SWN and LWN the net shortwave and longwave fluxes, SHF and LHF the sensible and latent heat fluxes, G the heat transfer through the snow. SWN (Eq. 2.6) and LWN (Eq. 2.8) are computed as the difference between downwelling (SWD or LWD) fluxes from the radiative scheme and the upwelling fluxes (SWU and LWU). SWU (Eq. 2.7) is defined as

SWD energy reflected by the surface albedo (α), while LWU (Eq. 2.9) is defined by the Stefan-Bosman Law (surface emissitivy (ε) times Stefan-Bosman constant (σ) times the fourth power of the surface temperature (ST)).

Since MAR does not represent the penetration of radiative fluxes into the snowpack, the energy budget for inner layers only depends on G that represents heat transfer with adjacent (above and below) layers, or for the deepest layer with the ground or SST below the sea-ice. The sub-grid SST beneath sea ice is fixed at -2 °C while the sea-ice surface temperature is free to evolve according to its surface energy balance. Snow-covered surface temperature is limited at 0 °C and any excess of energy ($SEB > 0$) is used to melt snow (Lefebre et al., 2003). On the opposite, any deficit in surface energy ($SEB < 0$) is compensated by (re)freezing liquid water (melt and rain). Liquid water can percolate through the snowpack depending on its permeability (Colbeck, 1972). In the Antarctic configuration, each snow/firn layer has a maximum water retention of 5%. The liquid water saturates each successive vertical layer as long as the underlying layer is permeable ($\rho < 830\,\mathrm{kg\,m^{-3}}$). Remaining liquid water beyond the snowpack saturation is converted into surface runoff. In the absence of a water-routing hydrological scheme and as Zuo and Oerlemans (1996) runoff delay is not activated over the AIS (unlike Greenland), all surface water that could potentially form melt ponds is considered as runoff, i.e., is instantaneously lost by the ice sheet.

The albedo of the ice sheet depends on the optical properties of snow, the thickness of the snow cover, the presence of blue ice, meltwater and clouds. The penetration of solar radiations in the snow strongly differs according to the spectral wavelength. The snow albedo (α_s) is therefore computed in three spectral bands (0.3-0.8 µm, 0.8-1.5 µm and 1.5-2.8 µm) to represent different solar absorption (Brun et al., 1989). However, since the radiative scheme outputs are broadband radiations, the snow albedo (Eq. 2.10) is a weighted average of the albedo in the three spectral bands:

$$\alpha_s = 0.6 \cdot \alpha_{0.3-0.8\mu m} + 0.3 \cdot \alpha_{0.8-1.5\mu m} + 0.1 \cdot \alpha_{1.5-2.8\mu m}, \qquad (2.10)$$

where α_s is the broadband snow albedo, and $\alpha_{0.3-0.8\mu m}$ (Eq. 2.11), $\alpha_{0.8-1.5\mu m}$ (Eq. 2.12), $\alpha_{1.5-2.8\mu m}$ (Eq. 2.13) are a function of the optical grain size (Brun et al., 1992) and successively modified in Lefebre et al. (2003) and Alexander et al. (2014):

$$\alpha_{0.3-0.8\mu m} = max(0.94, 0.96 - 1.58 \cdot \sqrt{d}), \qquad (2.11)$$

$$\alpha_{0.8-1.5\mu m} = 0.95 - 15.4 \cdot \sqrt{d}, \qquad (2.12)$$

$$\alpha_{1.5-2.8\mu m} = 346 \cdot min(d, 0.0023) - 32.1 \cdot \sqrt{d} + 0.88, \qquad (2.13)$$

The optical grain size d (m) is a function of snow grain properties (Brun et al., 1992). While faceted crystals have a lower optical grain size than spherical snow grains, larger snow grains notably induced by melt decrease the albedo (Lefebre et al., 2003). However, the snow albedo cannot be lower than 0.7. This value represents the albedo of snow that has previously melted. The minimum firn albedo (Eq. 2.14) during the transition from snow to ice is a function of the firn density (ρ) (Tedesco et al., 2016) and is comprised between 0.55 and 0.7:

$$\alpha_{firn} = 0.55 + (0.7 - 0.55) \times (\rho - 920)/(450 - 920), \qquad (2.14)$$

Over the AIS, the albedo of blue-ice areas in MAR can vary between a minimum ($\alpha_{icemin} = 0.5$) and a maximum value ($\alpha_{icemax} = 0.55$) depending on the presence of meltwater at the surface (Eq. 2.15):

$$\alpha_{ice} = \alpha_{icemin} - (\alpha_{icemin} - \alpha_{icemax}) \times e^{-\sqrt{(RU/K)}}, \qquad (2.15)$$

with RU the amounts of accumulated melt water that will runoff (unit: $\mathrm{kg\,m^{-2}}$), and K a scale factor set to 60 ($\mathrm{kg\,m^{-2}}$). However, as the delay of runoff is switched off, $\alpha_{ice} = \alpha_{icemax}$ in our configuration.

In case of a snow cover thickness (h_{snow} in m) thinner than 0.1 m, the albedo reflects the contribution of both snow (α_s) and ice (α_{ice}) albedos (Lefebre et al., 2003) (Eq. 2.16) while the albedo is the snow albedo for thicker snow cover. Furthemore, SISVAT takes into account the effect of solar zenith angle on the snow albedo as formulated by Segal et al. (1991) and the increase in albedo due to clouds that absorbs solar radiation in the same near-infrared spectrum than snow following Greuell and Konzelmann (1994).

$$\alpha = (\alpha_s \times h_{snow}) + (\alpha_{ice} \times (0.1 - h_{snow}))/0.1, \qquad (2.16)$$

SISVAT only simulates a limited number of snow layers and therefore uses a sophisticated aggregation scheme to discretise the snowpack in several (maximum

fixed) layers. An aggregation scheme (described in Brun et al. (1989, 1992) manages the stratification of the snowpack due to snow accumulation, ablation, settling, and metamorphism enabling the dynamical evolution of the physical properties of the different layers though time. It merges layers having similar properties (metamorphism state, temperature, density, and water content) to conserve a maximum of 30 snow/ice layers in case of accumulation (snowfall and deposition). In the same way, the scheme splits the snowpack to ensure a minimal number of 10 layers over permanent-ice areas. Furthermore, the maximum layer thickness of the 4 uppermost layers is fixed (0.02, 0.05, 0.1, and 0.3 m) warranting a fine discretisation to represent surface-atmosphere interactions and sub-surface processes such as heat transfer. Ablated snow mass is removed from the uppermost layer. Finally, the internal snow layers cannot be thinner than 2 mm, and the fresh fallen snow mass is only added into the snowpack if the snowfall amount is larger than 1 mm for numerical stability reasons. Note that properties (such as metamorphism and inherent albedo) of the uppermost layer already take into account the fresh snowfall characteristics while the snow mass is added in the next precipitation event (Lefebre et al., 2003).

Drifting snow

Finally, another important climate feature of polar ice sheets is the wind-driven erosion of snow particles, subsequent transport and redeposition. Drifting snow can change local accumulation (Eisen et al., 2008), but also near-surface atmospheric properties (Le Toumelin et al., 2020). MAR includes a drifting-snow scheme that simulates wind-driven erosion based on Gallée et al. (2001) but did not accurately represent both SMB and drifting-snow events simultaneously at that time (Gallée et al., 2001; Gallée et al., 2005, 2013; Amory et al., 2015). The drifting-snow scheme has therefore been deactivated in many studies (e.g., Fettweis et al., 2017; Agosta et al., 2019; Fettweis et al., 2020; Mottram et al., 2020) including this work (and related publications (Kittel et al., 2018, 2020)). However, recents developments have enabled the reconciliation of the representation of both SMB and drifting-snow events (Amory et al., 2020). Although not used in the main part of this manuscript, the new drifting-snow scheme will be presented hereafter to complete the MAR presentation but also because part of the thesis was devoted to participating in the development and evaluation of this scheme on Adelie land, and then also over the AIS. This section is a summary of the exhaustive description of the new drifting-snow scheme developments that has been submitted to the *Geoscientific Model Development* Journal:

Amory, C., **Kittel, C.**, Le Toumelin, L., Agosta, C., Delhasse, A., Favier, V., and Fettweis, X.: Performance of MAR (v3.11) in simulating the drifting-snow climate and surface mass balance of Adelie Land, East Antarctica, *Geosci. Model Dev. Discuss.* [preprint], in review, 2020.

Snow erosion is assumed to occur when the wind shear stress (the friction velocity) exceeds the cohesive and gravitational forces of the surface (the threshold friction velocity) represented in MAR as a function of the surface snow density only (Amory et al., 2020). The scheme computes the concentration of snow particles that are assumed to become mobile and bounce on the surface. This concentration represents the particle mass transported in saltation ($qsalt$) and is directly related to the difference between the friction velocity and the threshold friction velocity following Bintanja (2000), i.e, to what extent the shear stress overcomes the resistives forces maintaining the snow particles on the surface. The saltating particle concentration $qsalt$ is only theoretical and is used as a boundary condition for the diffusion of snow particles towards the suspension layer. This transport mode refers to the transport of snow particles without periodic contact with the surface, which is in MAR the snow advection occuring at the lowest atmospheric level. The diffusion of snow particles from the saltation layer (ie, theoretical level located at the surface in MAR) to the suspension layer (lowest atmospheric level) is a function of the difference between q_s (snow concentration at the lowest atmospheric level including both drifting and precipitation snow particles) and $qsalt$ (Gallée et al., 2001; Gallée et al., 2005; Amory et al., 2020). The drifting-snow model aims to represent the turbulent diffusion of eroded snow particles from the surface towards the atmosphere (Gallée et al., 2001).

Since the current version MAR does not distinguish drifting snow originated from the surface and snow resulting from cloud precipitation, q_s represents both types of snow. Snow is then drag vertically and horizontally by the turbulent, cloud-microphysical and advection schemes where snow can interact with solar radiations and the surrounding atmosphere especially by sublimating, which in turns modify the humidity and energetic bilan of atmospheric layers as described above.

Drifting-snow particles also induce modifications in surface properties. Re-petition of erosion and deposition events increase the snowpack cohesion (Vionnet et al., 2013) and changes grain properties from dendritic to rounded shapes (Sato et al., 2008). Furthermore, erosion and deposition creates microrelief (sastrugis) determining the roughness of snow surfaces (e.g., Amory et al., 2017). When

the drifting-snow scheme is switched on, MAR takes into account these processes by prescribing different surface properties (fallen-snow density, metamorphism and roughness length) than the parameterisations used in the version without drifting-snow. For instance, the increase in snowpack cohesion is represented by a progressive increase in density of the fresh snow reaching the surface replacing the density equation (Eq. 2.4 presented above (Amory, 2020) while the parameterisation of surface roughness depends on the temperature as proposed by Amory et al. (2017).

An important limit of the current drifting-snow scheme implemented in MAR is the non-distinction of the snow particles source between the surface and the clouds. This means that MAR outputs with drifting snow prevent analysis of changes resulting from separate trends in drifting-snow or cloud-created precipitation. Furthermore, the drifting-snow contribution to surface properties (density, grain sizes and shapes) is only assessed through an assumption of its relative importance compared to cloud-created precipitation. Finally, MAR assumes the same sedimentation velocity for both drifting and cloud-created snow particles, while due to their smaller size, drifting-snow particles should have a lower sedimentation velocity (Gallée et al., 2005) potentially underestimating their residence time in the atmosphere and the related interactions. Future developments of the drifting-snow scheme should therefore focus on this aspect. This requests a radical modification of the previously described scheme to add an additional hydrometeor, as already done in the future MAR version (Gallée, 2020).

2.1.4   Common set-up and versions

In this manuscript, two different versions of MAR adapted to the AIS are used: the version 3.6.4 (described in Agosta et al. (2019)) for Ch. 4 and the version 3.11 (presented in Kittel et al. (2020)) for Ch. 5 and Ch. 6. Furthermore, Chapter 4 relies on a coarse resolution (50km) as a consequence of the large number of simulations that were carried out while MAR simulations were performed at a 35km resolution for Ch. 5 and Ch. 6. A comparison of the results from these two different versions (and resolutions) is presented in Ch. 3 and shows that the MAR performances are similar across this manuscript despite using different resolutions and versions.

The Antarctic topography, and ice/rock fractions are computed from the 1 km resolution digital elevation model Bedmap2 (Fretwell et al., 2013). The ice